Microscopic Properties of the Pinwheel Kagome Compound $Rb_2Cu_3SnF_{12}$

M. S. Grbić,[1,2,*] S. Krämer,[1] C. Berthier,[1] F. Trousselet,[3] O. Cépas,[3] H. Tanaka,[4] and M. Horvatić[1,†]

[1]*Laboratoire National des Champs Magnétiques Intenses, LNCMI—CNRS (UPR3228), UJF, UPS, and INSA, BP 166, 38042 Grenoble Cedex 9, France*

[2]*Department of Physics, Faculty of Science, University of Zagreb, P.O. Box 331, HR-10002 Zagreb, Croatia*

[3]*Institut Néel, CNRS and Université Joseph Fourier, BP 166, 38042 Grenoble Cedex 9, France*

[4]*Department of Physics, Tokyo Institute of Technology, Meguro-ku, Tokyo 152-8551, Japan*

(Received 5 November 2012; revised manuscript received 31 March 2013; published 12 June 2013)

Using ^{63,65}Cu nuclear magnetic resonance in magnetic fields up to 30 T, we study the microscopic properties of the 12-site valence-bond-solid ground state in the "pinwheel" kagome compound $Rb_2Cu_3SnF_{12}$. We find that the ground state is characterized by a strong transverse staggered spin polarization whose temperature and field dependence points to a mixing of the singlet and triplet states. This is further corroborated by the field dependence of the gap $\Delta(H)$, which has a level anticrossing with a large minimum gap value of $\approx\Delta(0)/2$, with no evidence of a phase transition down to 1.5 K. By the exact diagonalization of small clusters, we show that the observed anticrossing is mainly due to staggered tilts of the g tensors defined by the crystal structure and reveal symmetry properties of the low-energy excitation spectrum compatible with the absence of level crossing.

DOI: 10.1103/PhysRevLett.110.247203 PACS numbers: 75.10.Jm, 75.10.Kt, 75.25.−j, 76.60.−k

Frustrated magnetic systems attract a lot of interest due to the interplay of frustration and quantum effects that bring about the emergence of many exotic ground states and fractionalized excitations [1,2]. The ($S = 1/2$) Heisenberg model on the kagome lattice has a particularly high level of frustration leading to a nonmagnetic ground state and many competing singlet states at low energy [3]. The nature of the ground state is currently highly debated [4]. Proposals include various quantum spin liquids with unbroken lattice symmetry and valence bond solids (VBS) where the lattice symmetry is broken. Unfortunately, only a handful of real systems do not magnetically order at low temperatures, and not all of them are well suited to study the properties of their ground states. Even fewer can be grown as single crystals and without the intrinsic disorder that complicates the interpretation of experimental results.

Recently, a singlet ground state was found in the distorted kagome system $Rb_2Cu_3SnF_{12}$ [5], where the $S = 1/2$ spin is carried by the copper Cu^{2+} ion enclosed in an F_6 octahedron. The distortion of the kagome lattice can be seen as six elongated hexagons surrounding a regular one, and the spins are connected through the Cu^{2+}–F^-–Cu^{2+} bonds with four different bonding angles, creating four different exchange couplings. Magnetization measurements at high magnetic fields showed a crossover in the behavior of the system appearing between 10 and 20 T for the magnetic field perpendicular to the kagome planes ($\mathbf{H} \parallel c$ axis) and a gradual filling of the triplet band. It was proposed [6] that the strongest coupling ($J_1 =$ 216 K [7]) creates valence bonds between spin pairs and forms a "pinwheel" pattern around the regular kagome hexagon, with 12 sites in the unit cell (inset to Fig. 1). The remaining three couplings ($J_2 = 0.95J_1$, $J_3 = 0.85J_1$, $J_4 = 0.55J_1$) are somewhat weaker, and what remains of the pure kagome physics is an open question. It is important to note that, for the pure kagome model, a VBS state with a 12-site unit cell was originally described as resonating between the two pinwheel patterns [8]. It was argued that the distortions observed in $Rb_2Cu_3SnF_{12}$ stabilize the VBS with a single pinwheel pattern [6], and such chirality breaking has been recently predicted to occur spontaneously in the pure kagome model [9]. A neutron-scattering study [7] has found evidence of a 12-site VBS ground state, separated from the first triplet state with strongly renormalized energy gap $\Delta(H = 0) = 27$ K $\approx J_1/8$. Measurements in magnetic field up to 6 T applied along the c axis (perpendicular to the kagome planes) show a reduction of the singlet-triplet gap and lifting of the triplet band degeneracy, accounted for by a *longitudinal* Dzyaloshinskii-Moriya (DM) interaction ($\mathbf{D} \parallel c$) [7], which does not break the rotational U(1) symmetry.

The availability of $Rb_2Cu_3SnF_{12}$ in the form of large single crystals has already stimulated fruitful experimental and theoretical work [5–7,10,11]. However, the microscopic properties of the 12-site pinwheel VBS ground state as well as its behavior at high magnetic field are still unknown. In this Letter, we report an NMR study of the on-site copper ^{63,65}Cu nuclei in magnetic fields up to 30 T, applied parallel to the c axis (experimental details can be found in the Supplemental Material [12]). We find evidence of an unconventional magnetic lattice with strong staggered *transverse* magnetic moments. We determine the field dependence of the singlet-triplet gap and show that there is no phase transition connected with the closing of the gap, but rather a level anticrossing that keeps the gap open. Together with the field dependence of local spin

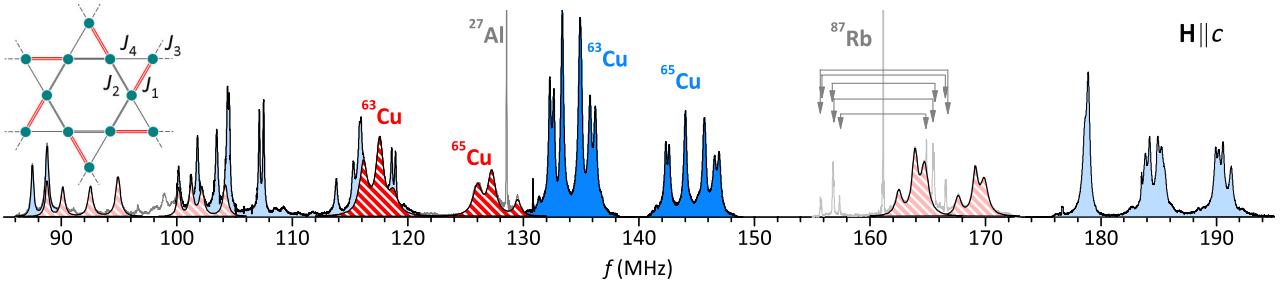

FIG. 1 (color online). ^{63,65}Cu spectrum of $Rb_2Cu_3SnF_{12}$ measured at 2.6 K and 11.568 T for the magnetic field parallel to the c axis of the crystal. Colors and their hues are used to distinguish positively (red hatched) and negatively (blue) polarized sites as well as the central lines (dark color) and satellites (light color). Additional lines of ^{87}Rb and ^{27}Al (used for magnetic field calibration) are marked in gray. The inset shows the exchange couplings structure of a pinwheel cluster.

polarizations, this points to a mixing of the singlet and triplet states, typically associated with DM interaction *perpendicular* to the field and/or a staggered off-diagonal g-tensor component g_s, that both break the U(1) rotational symmetry. We argue that the very existence of the anticrossing imposes an additional symmetry condition on the lowest triplet state, which defines the sign of the longitudinal DM interaction. By using exact diagonalization of small clusters, we show that the amplitude of the anticrossing gap is dominantly due to g_s terms.

When a single crystal sample is placed in a magnetic field, the NMR spectrum of the copper ^{63,65}Cu (spin 3/2) nuclei will show three lines per isotope for each nonequivalent site: one central line surrounded by two satellites. This sextuplet of lines is multiplied by the number of inequivalent sites; e.g., the spectrum shown in Fig. 1 presents a very complicated structure spanning over 100 MHz, consisting of 72 NMR lines originating from 12 sites. To analyze such spectra, we follow closely the procedure and nomenclature used in Ref. [13], where the technical details are in the second column of page 2. The six NMR frequencies of each sextuplet of lines belonging to one copper site are determined by the quadrupolar coupling tensor, described by its principal component ν_Q and the asymmetry parameter η, by the Zeeman coupling to the local magnetic field $H_{\rm eff}$, and by the (ϑ, φ) angles defining relative direction of that field with respect to the principal axes of the quadrupolar tensor. Here, these five parameters are further constrained by the known nuclear quadrupolar frequency $\nu_{\rm NQR} = \nu_Q\sqrt{1+\eta^2/3}$, as four different $\nu_{\rm NQR}$ frequencies, all in the narrow range of 49.8–55.3 MHz, have been reported in a previous study [14]. The main difficulty in the analysis of the spectra lies in the assignments of different sextuplets to lines in the NMR spectrum. This requires numerous trials and errors, where the correct assignment was recognized by successful fit to several complete spectra taken at different field values, leading to reasonable values of the fit parameters $(H_{\rm eff}, \vartheta, \varphi, \nu_Q, \eta)_i$, where i denotes different Cu sites. In particular, for nearly all the sites we found $\vartheta \approx 24° \pm 2°$ (while only two sites have somewhat smaller values $13° \pm 2°$), which corresponds precisely to what is expected from the crystal structure [5]. That is, for all CuF_6 octahedra, the (average) planes passing through four tetragonally placed F^- ions that define the $d_{x^2-y^2}$ orbital of copper are tilted by 22°–23° with respect to the kagome plane (see inset to Fig. 4).

Among the complete set of parameters, only the $H_{\rm eff}$ values are expected to be temperature (T) and field dependent. Once determined, the other parameters can be taken as constants, so that in the study of T and H dependence of spectra, from each NMR line position we can calculate the corresponding $H_{\rm eff}$ value. For these studies, we have thus measured only the central lines of the spectra, meaning that each Cu site was represented by two lines from the two ^{65,63}Cu isotopes, which should lead to the same $H_{\rm eff}$ value. As shown in Figs. 2(a) and 3(a), this is indeed the case. In these figures, we have plotted the negative of the local field $-H_{\rm loc} = H - H_{\rm eff}$, where H is the applied field, which is directly proportional to the local spin polarization $-H_{\rm loc} = -\mathbf{A} \times 2\langle \mathbf{S} \rangle - K_{\rm orb}\mathbf{H}$ up to relatively small constant correction due to the orbital contribution, estimated as $K_{\rm orb} \approx 1.5\%$. Typical values of the hyperfine coupling tensor $\mathbf{A}$ for the Cu nuclei in the CuF_6 environment are known [15], $A_\parallel \approx -18$ T, $A_\parallel/A_\perp \approx 10$, where "$\parallel$" denotes the principal axis of the $\mathbf{A}$ tensor, expected to be nearly parallel to the principal axis of the quadrupolar coupling tensor, i.e., tilted by $\approx \vartheta$ from $\mathbf{H} \parallel c$. In this case, both the longitudinal coupling constant $A_{zz} = A_\parallel \cos^2\vartheta + A_\perp \sin^2\vartheta$ as well as the transverse one $A_{z\perp} = 1/2(A_\parallel - A_\perp)\sin 2\vartheta \cos\phi$ are known, and the measured $-H_{\rm loc}$ directly reflects the corresponding local spin polarization $(S_z, S_\perp, \phi)$, where ϕ denotes the azimuthal angle relative to the one defined by the ϑ-tilted $A_\parallel$ axis. It is clear that from one number, $H_{\rm loc}$, one cannot *a priori* deduce three spin components. The necessary information to get S_z and $S_\perp$ spin components is thus obtained from the analysis of the $-H_{\rm loc}(T, H)$ dependence (Figs. 2 and 3).

Our NMR spectrum shown in Fig. 1 has a large number of lines, corresponding to many different local fields originating from crystallographically and/or magnetically different sites. In contrast to that, the room temperature

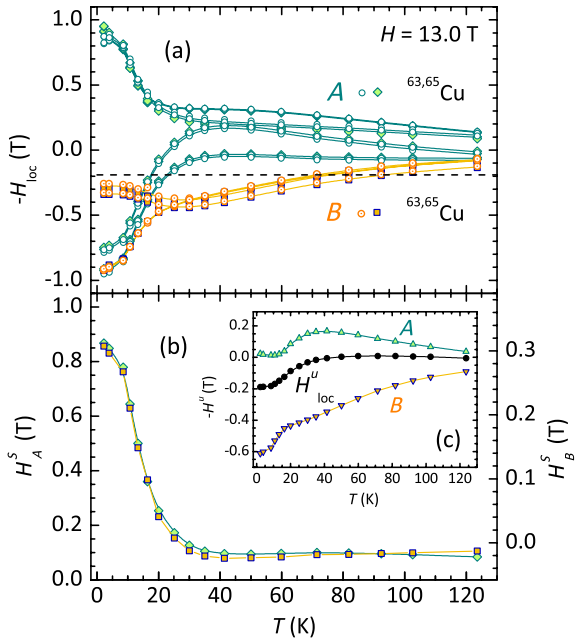

FIG. 2 (color online). (a) Temperature dependence of the local fields at 13.0 T. Two groups of sites are marked by the green (A) and orange (B) symbols, as defined in the legend. Circles (diamonds and squares) show the values obtained for ^{63}Cu (^{65}Cu) isotope. The dashed line marks the estimated orbital contribution ($K_{\rm orb} \approx 1.5\%$). (b) The average local *staggered* field at sites A (diamonds, left scale) and B (squares, right scale). (c) The *uniform* hyperfine field averaged over the A, B and all sites (up triangles, down triangles, and solid circles, respectively).

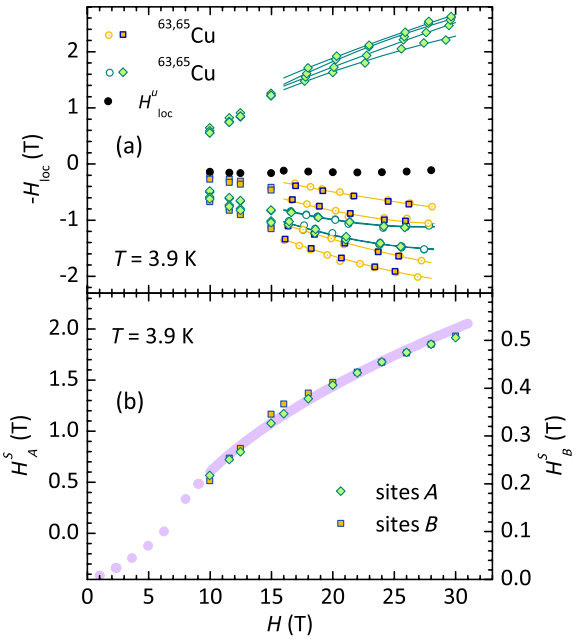

FIG. 3 (color online). (a) Magnetic field dependence of the local fields at 3.9 K, with the same symbol and color code as in Fig. 2. (b) The average local staggered field. The thick line is a guide for the eye showing approximately a square-root dependence, whereas the dotted line shows an expected qualitative behavior for lower magnetic fields.

crystal structure predicts only *two* inequivalent copper sites in the unit cell. In order to understand the origin of the observed distribution of local fields, we have tracked their temperature dependence, shown in Fig. 2(a). There, one can identify two families of sites [marked with A (green) and B (orange)] occupied in the ratio $P(A)$:$P(B) = 8$:$4 = 2$:1, which can be associated with 12 sites per unit cell of the crystal structure below 215 K. Close to this temperature a small structural distortion has been observed by x-ray scattering [7], leading to the enlargement of the lattice cell to $2a \times 2a$, but the superlattice peaks were too weak to fully resolve the new structure at lower T. While this structural transition was not detected in the dc susceptibility, such subtle deformations can cause the splitting of the NMR lines. Furthermore, in Fig. 2(a) it is easy to observe the local "pairs" of each family that develop opposite polarizations at low temperature, thus defining the local staggered ($H^s_{A,B}$) and uniform ($H^u_{A,B}$) fields

$$H^s_{A,B} = (\langle H_{i+}\rangle_{A,B} - \langle H_{i-}\rangle_{A,B})/2,$$
$$H^u_{A,B} = (\langle H_{i+}\rangle_{A,B} + \langle H_{i-}\rangle_{A,B})/2, \quad (1)$$

where the average is taken over the upper (H_{i+}) or lower (H_{i-}) local fields of either A or B family of lines.

In Fig. 2(b), we can see that both A and B sites develop very strong staggered moments below 30 K [$\approx\Delta(0)$]. Additionally [see Fig. 2(c)], the two families of lines also develop distinct positive (H^u_A) and negative (H^u_B) uniform magnetizations. When T is raised, the distribution of the local fields is reduced but retains a finite value, even at 120 K [$\approx 4\Delta(0)$] [16]. This site inequivalence is attributed to the previously mentioned structural distortion of the lattice [7]. On the other hand, the development of the staggered and uniform fields at temperatures below the zero field gap in Fig. 2(b) is clearly related to the formation of the local spin order.

As already mentioned, both the transverse and longitudinal magnetization contribute to $H_{\rm loc}$ and, because of the uncertainty in the site environments and the complexity of the spectra, we could not find a way to formally separate the two contributions. However, considering their relative size at low temperature $|H^s| \gg |H^u|$, it is natural to associate the staggered (uniform) fields $H^{s(u)}$ defined by Eqs. (1) to the transverse (longitudinal) local spin polarization $S_\perp (S_z)$, respectively. This is further supported by the field dependence of these values and the physics behind them, as discussed later. Within this attribution we find very large low-T values for the local transverse staggered spin polarization, $S_\perp \cos\phi \approx 14\%$ and 6% for the A and B sites, respectively, whereas the local uniform fields correspond to much smaller spin polarization of $S_z \approx 1.2\%$ and -2%. While in this way only a projection $S_\perp \cos\phi$ is

determined, in all cases the spins polarizations lie nearly completely in the kagome plane, $S_\perp \gg |S_z|$.

We observe that the total average $\langle S_z \rangle$ component is almost fully canceled out, $P(A)\langle S_z\rangle_A + P(B)\langle S_z\rangle_B \approx 0$, but the true value cannot be precisely defined, because of the uncertainty in the estimate of the orbital shift $K_{\rm orb}$ defining the zero. As regards the transverse staggered components, the smaller value of H_B^s for sites B can be explained either as weaker polarized moments having equivalent orientations $\phi_A \approx \phi_B$ or moments of similar size but with different ϕ values, e.g., $\phi_A \approx 0°$ and $\phi_B \approx 65°$. We cannot differentiate between these two cases, but the existence of a large staggered magnetization within the kagome planes is not affected by this uncertainty.

We have also followed the magnetic field dependence of the local polarizations up to 30 T (Fig. 3), measured at 3.9 K where the temperature dependence of the spin polarizations saturates. The field dependence of $H_{A,B}^s$ [Fig. 3(b)] is clearly different from the high field magnetization [5] and follows approximately a square-root dependence, reaching at 30 T a polarization of $S_\perp \cos\phi \approx 30\%$ for the A sites. Similar temperature and magnetic field dependence of local moments was found [17] in $SrCu_2(BO_3)_2$, another two-dimensional frustrated dimer system. There, a moderate in-plane DM interaction ($D/J = 0.034$) and $g_s(=0.023)$ terms were enough to mix the singlet and triplet states and thus create considerable transverse staggered moments, while the longitudinal moments remained much smaller. In $Rb_2Cu_3SnF_{12}$, the DM interaction is estimated to be much stronger ($D/J = 0.18$–0.2) [7,10], but only the longitudinal c-axis component of the **D** vector, which does *not* induce level mixing, has been considered so far.

While the application of the critical field in spin-dimer systems is expected to close the singlet-triplet gap by the level crossing, leading to a new polarized phase, mixing of the singlet and triplet states will keep the gap open (''anticrossing''). In order to follow the magnetic field dependence of this gap, we have performed measurements of the nuclear spin-lattice relaxation rate T_1^{-1}, which probes the dynamics of the low-energy excitations. Importantly, no qualitative changes in the spectra nor any T_1^{-1} anomaly were observed down to 1.5 K, confirming the absence of a phase transition. For a fixed field, the temperature dependence of T_1^{-1} below 6 K (top inset of Fig. 4) shows an activated behavior $\propto e^{-\Delta(H)/T}$ typical of a two-magnon process, allowing us to determine the value of the gap $\Delta(H)$ [18]. As the field is raised from 8 to 13 T, the gap value is seen to decrease (Fig. 4), and the NMR data smoothly continue those determined from the neutron scattering up to 6 T [7]. Close to 13 T, the gap value passes through a broad minimum after which it again increases at higher fields. The residual value of the gap $\Delta(13\ \mathrm{T}) \approx \Delta(0)/2$ appears to be very large, which is clear evidence for important U(1)-symmetry-breaking terms that induce level anticrossing.

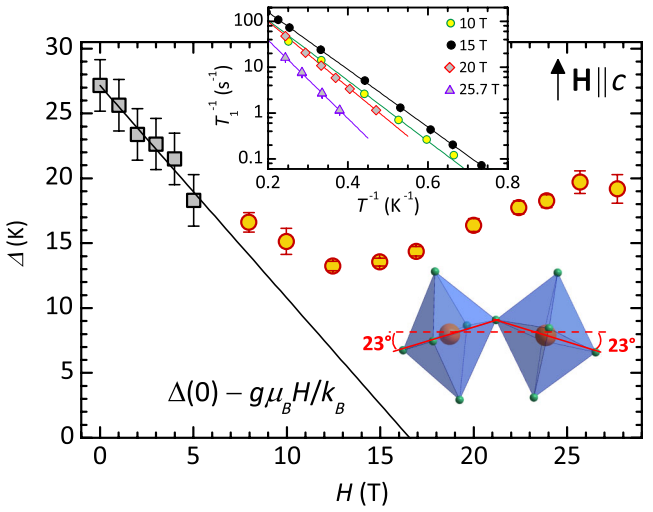

FIG. 4 (color online). H dependence of the singlet-triplet energy gap measured by T_1^{-1} (red-yellow circles) and by neutron scattering (black-gray squares, from Ref. [7]). Insets: (top) Arrhenius plot of the measured $T_1^{-1}(T)$ dependence (symbols) and the fit (lines) used to extract the gap values shown in the main figure. Only selected, representative data sets are shown. (bottom right) Two neighboring CuF_6 octahedra.

In order to describe this anticrossing, we have included the transverse anisotropies in the Hamiltonian, which was defined previously by the Heisenberg couplings $J_1 - J_4$ and the z component (d_z) of the **D** vector [7,10], and performed exact diagonalizations of this Hamiltonian on clusters of $N = 12$ and 24 sites (Supplemental Material [12]). We consider the in-plane DM terms ($d_p = D_{\perp i}/J_i$) perpendicular to the bonds and respecting the crystal symmetry as well as the off-diagonal g-tensor terms as generated by the strong tilting of the CuF_6 octahedra, $\vartheta \approx 23°$ (inset of Fig. 4), leading to $g_s = 0.135$ (see the Supplemental Material [12] for definitions). Remarkably, depending on the helicity of these terms as compared to that defined by the screw axis of the d_z vector, the system presents either level crossing or anticrossing. That is, depending on the sign of d_z, the lowest triplet state will be either of E_g^+ or E_g^- symmetry, and only one of these two (in the present case E_g^- corresponding to $d_z > 0$, see the Supplemental Material [12]) allows for level anticrossing. The calculated gap presents *small* finite-size effects near the anticrossing, in contrast to the zero-field gap as described in Refs. [7,10]. This enabled us to make a theoretical estimate of the minimum gap size and position and conclude that the experimentally observed gap is well accounted for by the g_s terms alone, with calculated values 13.0 K and 14.0 T (Supplemental Material [12]), whereas only a minor contribution can come from d_p (estimated to $|d_p| < 0.012$).

In summary, we have described the microscopic properties of $Rb_2Cu_3SnF_{12}$ by on-site ^{63,65}Cu NMR.

In the field perpendicular to the kagome planes and at low temperature, the NMR spectra evidence a strong staggered transverse spin polarization, growing approximately as the square root of the magnetic field value. The field dependence of the singlet-triplet gap measured via the T_1^{-1} data presents an anticrossing of the energy levels with a large residual gap value $\Delta(13\ \mathrm{T}) \approx \Delta(0)/2$, well accounted for by the staggered g-tensor terms defined by the crystal structure. We have argued that the observed anticrossing and the absence of phase transition is only compatible with a given sign of d_z. The other sign would lead to a phase transition because the spontaneously induced transverse moments would break the rotation symmetry of the crystal. Further theoretical work is needed to fully exploit the available information on spin polarizations.

We acknowledge fruitful discussions with Y. Fukumoto, H. Mayaffre, and S. Maegawa. We thank W. G. Clark for reviewing the manuscript. Part of this work has been supported by the French ANR project NEMSICOM, by the EuroMagNET network under EU Contract No. 228043, by the ARRS Project No. J1-2118, and by the EU FP7 Project SOLeNeMaR No. 229390.

*mgrbic@phy.hr
†mladen.horvatic@lncmi.cnrs.fr

[1] B. Normand, Contemp. Phys. **50**, 533 (2009).
[2] L. Balents, Nature (London) **464**, 199 (2010).
[3] P. Lecheminant, B. Bernu, C. Lhuillier, L. Pierre, and P. Sindzingre, Phys. Rev. B **56**, 2521 (1997).
[4] See the discussion in S. Yan, D. A. Huse, and S. R. White, Science **332**, 1173 (2011) and references therein.
[5] K. Morita, M. Yano, T. Ono, H. Tanaka, K. Fujii, H. Uekusa, Y. Narumi, and K. Kindo, J. Phys. Soc. Jpn. **77**, 043707 (2008).
[6] B.-J. Yang and Y. B. Kim, Phys. Rev. B **79**, 224417 (2009).
[7] K. Matan, T. Ono, Y. Fukumoto, T. J. Sato, J. Yamaura, M. Yano, K. Morita, and H. Tanaka, Nat. Phys. **6**, 865 (2010).
[8] A. V. Syromyatnikov and S. V. Maleyev, Phys. Rev. B **66**, 132408 (2002).
[9] S. Capponi, V. R. Chandra, A. Auerbach, and M. Weinstein, Phys. Rev. B **87**, 161118(R) (2013).
[10] K. Hwang, K. Park, and Y. B. Kim, Phys. Rev. B **86**, 214407 (2012).
[11] E. Khatami, R. R. P. Singh, and M. Rigol, Phys. Rev. B **84**, 224411 (2011).
[12] See Supplemental Material at http://link.aps.org/supplemental/10.1103/PhysRevLett.110.247203 for experimental methods and details of exact diagonalization calculations and symmetry arguments.
[13] F. Aimo, S. Krämer, M. Klanjšek, M. Horvatić, C. Berthier, and H. Kikuchi, Phys. Rev. Lett. **102**, 127205 (2009).
[14] H. Tashiro, M. Nishiyama, A. Oyamada, T. Itou, S. Maegawa, M. Yano, T. Ono, and H. Tanaka, J. Phys. Conf. Ser. **320**, 012052 (2011).
[15] T. Kubo and A. Nozaki, Bull. Nara Univ. Educ. **35**, 31 (1986).
[16] The spectral lines were not observed at higher temperatures because the short spin-spin correlation time (T_2) strongly reduces the signal intensity.
[17] K. Kodama, S. Miyahara, M. Takigawa, M. Horvatić, C. Berthier, F. Mila, H. Kageyama, and Y. Ueda, J. Phys. Condens. Matter **17**, L61 (2005).
[18] All central NMR lines follow the same temperature dependence, meaning that the gap opens homogeneously in the system.

SUPPLEMENTAL MATERIAL

to 'Microscopic properties of the "pinwheel" kagome compound $Rb_2Cu_3SnF_{12}$' by M. S. Grbić *et al.*

Experimental methods

Transparent single crystals of $Rb_2Cu_3SnF_{12}$ were synthesized according to the procedure described in ref. [1]. The size of the crystal used for the NMR study was $3\times4\times1$ mm^3. The sample was placed in a silver-wire radio-frequency coil together with a small piece of thin aluminum foil, which was used to calibrate the value of the applied magnetic field H. The c axis of the crystal was oriented within 2° along the field, as confirmed from the angular dependence of the spectrum. A laboratory-made NMR spectrometer was used for the data acquisition; the spectra were recorded using a Hahn-echo pulse sequence, $\pi/2-\tau-\pi$, with typical π pulse value of 3 μs, and $\tau = 10$ μs. An inversion-recovery pulse sequence was used for measurements of the spin-lattice relaxation rate. The measurements in fields up to 17 T were made in a superconducting NMR magnet, while the data at higher field values were taken using a 20 MW resistive magnet at the LNCMI - Grenoble.

Anticrossing at high magnetic field in the pinwheel kagome $Rb_2Cu_3SnF_{12}$

We focus on the anticrossing observed in the field-dependence of the spin gap measured in $Rb_2Cu_3SnF_{12}$ and describe it by using a model that includes the transverse anisotropies expected in this compound.

In systems where the magnetization S^z is a conserved quantity, the energy gap between the ground state $|S^z = 0\rangle$ and the first triplet state $|S^z = 1\rangle$ decreases when an external magnetic field is applied along the z-axis and is expected to vanish once a critical field is reached. This triggers a phase transition that can be described as a Bose-Einstein condensation of magnons [2]. In real systems, weak transverse anisotropies of spin-orbit origin may mix the states with different S^z and lift the degeneracy at the crossing point, resulting in an anticrossing of the energy levels and preventing a true condensation. We show here that in the present case this may occur or not, depending on the symmetry of the lowest triplet state.

We consider a model previously introduced for $Rb_2Cu_3SnF_{12}$, with Heisenberg couplings and Dzyaloshinskii-Moriya (DM) interactions [3, 4]

$$\mathcal{H}_0 = \sum_{<i,j>} J_{ij}\mathbf{S}_i\cdot\mathbf{S}_j + \mathbf{D}_{ij}\cdot(\mathbf{S}_i\times\mathbf{S}_j) - gH\sum_i S_i^z \quad \text{(S1)}$$

where $\mathbf{S}_i$ is the $S = 1/2$ operator of the Cu^{2+} spin, H the external magnetic field along the z direction (along c axis, perpendicular to the kagome planes), and $g \equiv g_{cc} = 2.44$ the measured gyromagnetic factor. We recall that there are four inequivalent bonds in the 12-spin unit-cell, described by $J_{ij} = J_{n=1,...,4}$ (see Fig. S1). DM vectors are defined on oriented bonds in Fig. S1, and characterized by two amplitudes $d_z = D_{n,z}/J_n$ and $d_p = D_{n,p}/J_n$ $(n = 1, ..., 4)$ for the out-of-plane and in-plane components, respectively. The whole pattern of DM vectors can be deduced by using the C_3 rotation and the inversion at the middle of the pinwheel. As in previous studies, we also neglect the DM component along the bond, since the lattice distortions allowing for it remain weak in the Rb compound.

In addition, there are transverse magnetic fields (with staggered components) within the plane, generated by the off-diagonal elements $g_{z\perp}$ of the g tensor, corresponding to the tilts of the CuF_6 octahedra that define the principal axes of the g tensor (see the inset of Fig. 4). These terms can be included in the Hamiltonian as:

$$\mathcal{H} = \mathcal{H}_0 - g_s\,H\sum_i \hat{\mathbf{e}}_i\cdot\mathbf{S}_i, \quad \text{(S2)}$$

where $g_s = 0.135$ and the unit-vectors $\hat{\mathbf{e}}_i$ point in the direction of the tilt of the CuF_6 octahedra. They are determined by the crystal structure and shown for each site in Fig. S1, up to symmetry operations. g_s is the off-diagonal tensor component $g_s \equiv g_{z\perp} = (g_\parallel - g_\perp)\sin(2\vartheta)/2$, determined by the anisotropy of the principal-axis values, $g_\parallel$ and $g_\perp$, of the tensor (supposed to be axial, as is the quadrupolar tensor we determined by NMR), and by the tilt of the principal axis ($\vartheta = 23°$) with respect to the crystalline c axis. The estimate of this tilt angle comes from the crystal structure (tilt of the average coordination plane of 4 fluorine first neighbors; see the inset of Fig. 4) and from the corresponding tilt of the quadrupolar tensor, as explained in the manuscript. The experimental values $g_{cc} = 2.44$ and $g_{aa} = 2.15$, determined in Ref. [1], correspond to the rotated g tensor:

$$\begin{aligned} g_{cc} &= \cos^2(\vartheta)g_\parallel + \sin^2(\vartheta)g_\perp, \\ g_{aa} &= g_\perp/2 + [\sin^2(\vartheta)g_\parallel + \cos^2(\vartheta)g_\perp]/2, \end{aligned} \quad \text{(S3)}$$

where g_{aa} is the average over all of the in-plane (ϕ) directions. Inverting equations S3 leads to $g_\parallel = 2.497$ and $g_\perp = 2.121$. Thus, we obtain an anisotropy of 15 % for the g tensor, which characterizes the Cu^{2+} ion coordinated by 4 oxygen or fluorine ions (e.g., see [5]). The relatively large g_s value is then determined by the strong tilt angle ϑ.

It is important to observe that neither the in-plane DM interaction nor the transverse fields conserve the magnetization along the z-axis and, therefore, both may account for the anticrossing.

Perturbation theory in the inter-dimer couplings and non-S^z-conserving terms gives some insights into the properties of the low-energy states. At first-order, the

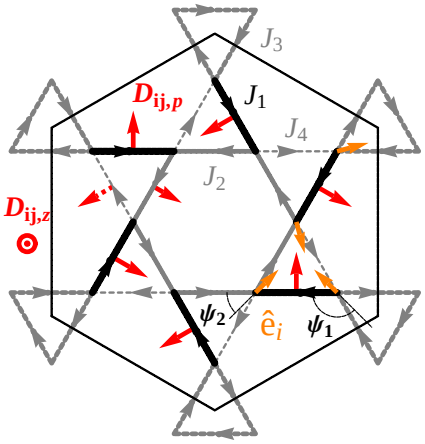

FIG. S1: Model of DM couplings (red arrows) and transverse magnetic fields (orange arrows) for the pinwheel kagome $Rb_2Cu_3SnF_{12}$ (not all vectors are shown but they can be deduced by symmetry; $\psi_2 = 51°$, $\psi_1 = 131°$). The unit-cell (hexagon) is also shown.

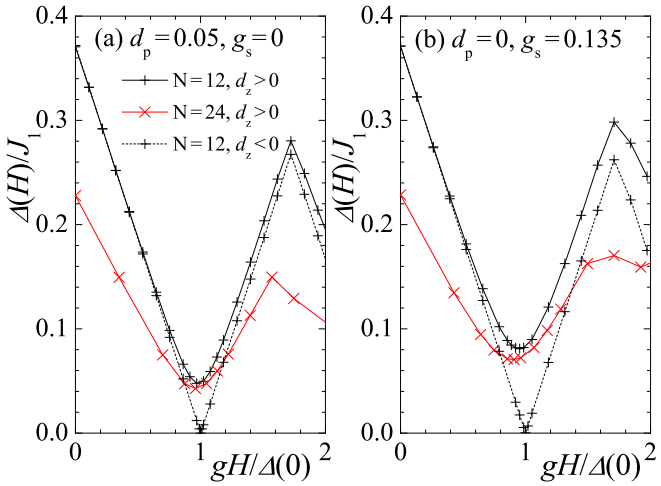

FIG. S2: Magnetic field dependence of the energy gap, $\Delta(H)$, calculated by exact diagonalization of the Hamiltonian, including transverse DM interactions (a) or transverse fields (b). The anticrossing (resp. crossing) is found for $d_z > 0$ (resp. $d_z < 0$), as explained by symmetry arguments.

ground state $|0\rangle$ is a product of singlets on the strongest bonds (coupling J_1 – there are six such bonds per unit cell) and the first excited state $|1\rangle$ is a $Q = 0$ state with one strong bond promoted to a triplet [3, 4]. The latter wave functions can be classified according to the irreducible representations of C_3 rotation, $A_{g,u}$ and $E_{g,u}$, where g and u denote even and odd wave-functions with respect to the inversion at the center of the pinwheel. d_z lifts the two-fold degeneracy of the $E_{g,u}$ modes into $E^{\pm}_{g,u}$ (corresponding to a $\pm 2\pi/3$ phase acquired upon $2\pi/3$ rotation), both having $S^z = \pm 1$, while the $S^z = 0$ states remain unchanged [3]. Changing the sign of d_z interchanges the + and − modes.

The level mixing is given by the matrix element $\langle 1|\mathcal{H}|0\rangle$. The state $\mathcal{H}|0\rangle$ is even under the inversion and picks up a $-2\pi/3$ phase under rotation, as imposed by the clockwise rotation pattern of the $\mathbf{D}_{ij,p}$ vectors, i.e. it transforms as E^-_g. Therefore the matrix element vanishes for all triplet states $|1\rangle$ except the one with E^-_g symmetry. E_g triplets are indeed predicted to be the two lowest energy states, with the splitting between E^+_g and E^-_g controlled by d_z [3, 4]. For $d_z > 0$ (resp. $d_z < 0$), the lowest triplet is that with E^-_g symmetry (resp. E^+_g) and there will be, therefore, an anticrossing (resp. a crossing). The experimental observation of an anticrossing is, therefore, only compatible with $d_z > 0$ (with the definition of Fig. S1). In other words, the lowest triplet state must have an E^-_g symmetry. This prediction, based on symmetry arguments, is expected to remain valid beyond perturbation theory, as we shall confirm next. Interestingly, it can be tested by other experimental probes, such as polarized neutron inelastic scattering or direct "forbidden" optical transitions between the ground state and the first excited state, as in $SrCu_2(BO_3)_2$ [6].

In order to test this prediction beyond perturbation theory and compute the gap in the relevant limit of strong interdimer couplings, we have computed the energy gap by exact diagonalizations of $\mathcal{H}$ for small clusters ($N = 12, 24$ spins). We have fixed the exchange couplings as previously extracted from neutron scattering measurements, $J_2 = 0.95J_1$, $J_3 = 0.85J_1$, $J_4 = 0.55J_1$ and $|d_z| = 0.18$ ($J_1 = 216$ K) [3].

We show in Fig. S2(a) the energy gap as a function of the field for finite transverse DM interaction. First, we find an anticrossing if $d_z > 0$, and a crossing if $d_z < 0$, confirming the symmetry argument given above. Second, for $d_z > 0$, the minimal value Δ_m of the gap at the anticrossing increases linearly, $\Delta_m/J_1 = 0.86d_p$ at small d_p. It is interesting to note that finite-size effects on Δ_m are small compared to those on $\Delta(0)$ and therefore allow us to estimate the anisotropic coupling. By using $\Delta_m = 13$ K, as determined by our NMR study, and $J_1 = 216$ K, and assuming the anticrossing would be caused by transverse DM interactions only, we would have $d_p = 0.07$.

However, as mentioned earlier, the staggered fields associated with the off-diagonal component of the g tensor g_s are also expected to produce an anticrossing (Fig. S2(b)). This occurs again only for $d_z > 0$ for the same reasons as before. For $N = 24$, and in the absence of in-plane DM components ($d_p = 0$), we find that $\Delta_m/J_1 = 0.522g_s$. As seen in Fig. S2(b), Δ_m tends to decrease when increasing the system size. A crude estimate of the finite-size effects based on the scaling $\Delta_m = \Delta^\infty_m + a/N$, leads to $\Delta^\infty_m/J_1 = 0.445g_s$. This gives $\Delta^\infty_m = 13.0$ K (for $g_s = 0.135$) in excellent agreement with the experimental result of 13 K. Furthermore, we can also perform the same finite-size scaling

on the positions of the minima in Fig. S2(b), which leads to $gH_m^\infty/\Delta(0) = 0.845$. From the experimental value $\Delta(0) = 27.2$ K we thus find $H_m^\infty = 14.0$ T, again in very good agreement with the experimental value of 13.3(5) T (see Fig. 4).

These estimates show that the strong tilting of the CuF_6 octahedra is itself sufficient to *quantitatively* account for the observed residual gap. If any in-plane component of the DM interaction exists, it should provide only a minor effect on the final size of Δ_m. Note that we cannot exclude that the $N = 24$ gap has already converged; the corresponding estimate of d_p value will then provide the upper bound. Assuming that the two effects are additive, as they are in the lowest order, $\Delta_m/J_1 = |0.522g_s + 0.86d_p|$ for $N = 24$, we find that $|d_p| < 0.012$, possibly compatible with zero. In a similar way (using $N \to \infty$ expressions), a reasonable estimate for the maximum error of $\pm 15\%$ in the determination of the g_s value leads to the same constraint $|d_p| < 0.012$.

We therefore conclude that the anticrossing is primarily caused by the g-tensor tilts, with in-plane DM interaction terms ($|d_p| < 0.012$) providing a minor correction to this effect. The anticrossing appears only if the helicity of the g-tensor tilts (here defined in Fig. S1) is the same as that defined by the screw axis d_z, that is if $d_z > 0$. It is interesting to note that the same g-tensor tilts with $d_z < 0$ would produce a (previously expected) level-crossing, and thus a sharp transition at the expected critical field value $H_c = \Delta(0)/g$.

[1] K. Morita, M. Yano, T. Ono, H. Tanaka, K. Fuji, H. Uekusa, Y. Narumi, and K. Kindo, J. Phys. Soc. Jpn. **77**, 043707 (2008).

[2] T. Giamarchi, C. Rüegg and O. Tchernyshyov, Nat. Phys. **4**, 198 (2008).

[3] K. Matan, T. Ono, Y. Fukumoto, T. J. Sato, J. Yamaura, M. Yano, K. Morita, and H. Tanaka, Nat. Phys. **6**, 865 (2010).

[4] K. Hwang, K. Park, and Y. B. Kim, Phys. Rev. B **86**, 214407 (2012).

[5] E. Buluggiu, G. Dascola, D. C. Giori, and A. Vera, J. Chem. Phys. **54**, 2191 (1971); Y. Fagot-Revurat, M. Horvatić, C. Berthier, P. Ségransan, G. Dhalenne and A. Revcolevschi, Phys. Rev. B **55**, 2964 (1997).

[6] O. Cépas and T. Ziman, Phys. Rev. B **70**, 024404 (2004).